



Orchestrated cellular, biochemical, and biomechanical optimizations endow platelet-rich plasma-based engineered cartilage with structural and biomechanical recovery

Ketao Wang^{a,c,e,1}, Ji Li^{a,1}, Yuxing Wang^{a,1}, Yaqiang Wang^d, Yuanyuan Qin^f, Fei Yang^{d,****}, Mingzhu Zhang^{c,***}, Heng Zhu^{b,**}, Zhongli Li^{a,*}

^a Department of Orthopedics, Chinese PLA General Hospital, Haidian, Beijing, 100853, China

^b Beijing Institute of Radiation Medicine/Beijing Institute of Basic Medical Sciences, Haidian, Beijing, 100850, China

^c Department of Foot and Ankle, Beijing Tongren Hospital, Capital Medical University, Beijing, 100730, China

^d Beijing National Laboratory for Molecular Sciences, Institute of Chemistry, Chinese Academy of Sciences, Beijing, 100190, China

^e Department of Orthopedic Surgery, Zhongshan Hospital, Fudan University, Shanghai, 200032, China

^f Department of Blood Transfusion, Chinese PLA General Hospital, Haidian, Beijing, 100853, China

ARTICLE INFO

Keywords:

Platelet-rich plasma
Cartilage regeneration
Structural recovery
Biomechanical recovery

ABSTRACT

Recently, biomaterials for cartilage regeneration has been intensively investigated. However, the development of scaffolds that capture regenerated cartilage with biomechanical and structural recovery has rarely been reported. To address this challenge, platelet-rich plasma (PRP)-based cartilage constructs with a well-orchestrated symphony of cellular, biochemical and biomechanical elements were prepared by simultaneously employing chondrogenic progenitor cells (CPCs) as a cell source, optimizing platelet concentration, and adding an enzyme-activator. It was shown that this triple-optimized PRP + CPC construct possessed increased biomechanical properties and suitable biochemical signals. The following *in vitro* study demonstrated that the triple-optimized PRP + CPC constructs generated cartilage-like tissue with higher expression levels of chondrogenic-specific markers, more deposition of cartilage-specific extracellular matrix (ECM), and greater biomechanical values than those of the other constructs. Twelve weeks after the construct was implanted in a cartilage defect *in vivo*, histological analysis, qPCR, and biomechanical tests collectively showed that the triple-optimized constructs yielded a more chondrocyte-like cell phenotype with a higher synthesis of Col-II and aggrecan. More importantly, the triple-optimized constructs facilitated cartilage regeneration with better biomechanical recovery than that of the other constructs. These results demonstrate the efficacy of the triple-optimization strategy and highlight the simplicity and potency of this PRP + CPC construct for cartilage regeneration.

1. Introduction

The repair of cartilage defects is still considered a clinical challenge, and cartilage tissue engineering has led to the development of several biomaterials for cartilage regeneration [1,2]. A variety of cartilage

substitute materials, such as protein-based matrices, bioactive ceramic scaffolds, and composite materials, have been explored [3–5]. However, there are still many difficult problems in treating cartilage defects with tissue engineering. One major problem is that the majority of bioengineering efforts fail to capture fully functional regenerated cartilage that

Peer review under responsibility of KeAi Communications Co., Ltd.

* Corresponding author. Department of Orthopedics, Chinese PLA General Hospital, Fuxing-Road, Beijing, 100853, China.

** Corresponding author. Department of Cell Biology, Beijing Institute of Radiation Medicine/Beijing Institute of Basic Medical Sciences, 27 Taiping Road, Beijing, 100850, China.

*** Corresponding author. Department of Foot and Ankle, Beijing Tongren Hospital, Capital Medical University, Beijing 100730, China.

**** Corresponding author. Beijing National Laboratory for Molecular Sciences, Institute of Chemistry, Chinese Academy of Sciences, 1st North Street, Zhong-guancun, Beijing, 100190, China.

E-mail addresses: fyang@iccas.ac.cn (F. Yang), mingzhuzhang@mail.ccmu.edu.cn (M. Zhang), zhudingdingabc@163.com (H. Zhu), lizhongli@263.net (Z. Li).

¹ K. Wang, J. Li, and Y. Wang contributed equally to this article.

<https://doi.org/10.1016/j.bioactmat.2021.03.037>

Received 16 October 2020; Received in revised form 18 March 2021; Accepted 19 March 2021

2452-199X/© 2021 The Authors. Publishing services by Elsevier B.V. on behalf of KeAi Communications Co. Ltd. This is an open access article under the CC

BY-NC-ND license (<http://creativecommons.org/licenses/by-nc-nd/4.0/>).

simultaneously facilitates biomechanical and structural recovery.

Recently, platelet-rich plasma (PRP) has attracted much attention for tissue engineering applications due to its low immunogenicity, high biodegradability, and cost-effectiveness [6,7]. In particular, as a pool of growth factors, PRP can provide endogenous growth factors and allow the transfer of nutrients within the material. Meanwhile, such biomimetic scaffolds can offer support for initializing the tissue repair process and provide conductive 3-dimensional (3-D) structures for cell migration and proliferation [7]. These characteristics provide PRP with potential to facilitate cartilage regeneration from the 3 primary aspects of tissue engineering: carrier/scaffold, cell resources, and bioactive factors. Nevertheless, PRP-based cartilage tissue engineering is faced with many challenges. First of all, selecting a favorable cell source is a crucial step in improving PRP-based cartilage tissue engineering due to its core role in administrating the synthesis of extracellular matrix (ECM) and the architecture of new tissue [8,9]. Additionally, achieving sufficient mechanical strength in PRP plays a critical role in creating and maintaining the biomechanics of newly regenerated tissue as well as in supporting tissue remodeling [10,11]. However, the high liquid content of PRP gels (nearly 90%) is generally accompanied by a poor biomechanical feature that largely hampers the applications of this soft material in cartilage regeneration, which highlights the necessity of

improving PRP strength [12]. Furthermore, growth factors at different concentrations yield discrepant effects on biological behaviors of cell sources, especially guiding them toward insufficient proliferation and undesirable differentiation [13–15]. However, PRPs with different platelet concentrations elicited evidently discriminatory growth factors within PRP gels [16]. Therefore, we need to capture a unique combination of favorable cell sources, reinforced PRP biomechanics, and optimized platelet concentrations to facilitate the structural and mechanical reconstruction of regenerated cartilage.

Recently, chondrogenic progenitor cells (CPCs) have gained increasing attentions as a potential cell source for tissue repairing due to their self-renewal, chondrogenesis potential, and migratory capabilities [17,18]. To pursue a suitable cell source for cartilage regeneration, we explored the intrinsic ability of CPCs, mesenchymal stem cells (MSCs), and chondrocytes to chondrogenic differentiation, and compared the effects of PRP on their proliferation and chondrogenesis *in vitro* and *in vivo* in our previous work. It was shown that CPCs possessed superior innate potential for chondrogenesis and exhibited a higher response to PRP stimulation over that of MSCs and chondrocytes [19]. Therefore, we hypothesized that CPCs could be applied as a favorable cell source in PRP-mediated cartilage tissue engineering.

Scaffolds can provide mechanical support for the initial regenerated

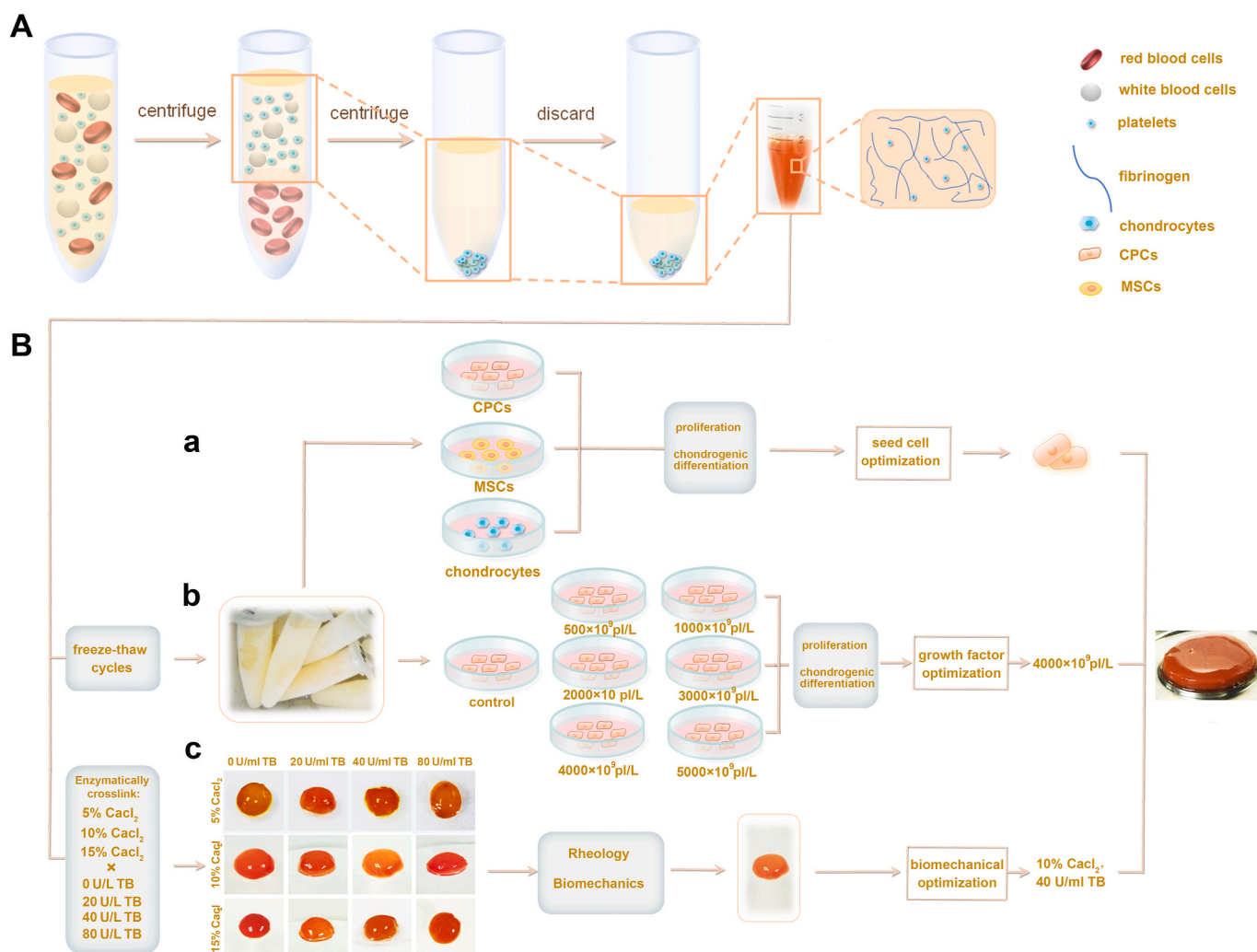


Fig. 1. Schematic diagrams of the fabrication of cellular, biochemical, and biomechanical triple-optimized PRP + CPC constructs. (A) Preparation of PRP through double centrifugation process. (B) Manufacturing the triple-optimized PRP + CPC constructs. (a) Compared the effects of PRP on CPC, MSC and chondrocyte proliferation, chondrogenesis and cartilage regeneration, and consequently selected CPCs as the superior cell source. (b) Optimization of platelet concentration for PRP constructs by assessing CPC proliferation, and differentiation post-stimulation of a series of PRPs of different concentrations. (c) Optimization of biomechanics for PRP constructs by using biomechanical tests and rheological assay.

tissue and contribute to the physiological evolution of the microstructure in the process of regeneration, so the biomechanical performance of the scaffold itself appears extremely important [20]. However, only a few studies to date have reported that PRP could achieve sufficient and controlled biomechanics in engineering constructs [21]. Thrombin can transform fibrinogen into fibrin, which is the core role in the coagulation and clotting formation processes [22]. Meanwhile, calcium ions (Ca^{2+}) are important participants in IX, X, XI, and thrombin activation in the coagulation process [23–26]. However, coagulation can be inhibited by an excessive Ca^{2+} , and anticoagulation occurs when the concentration is above 20 mmol/L [27,28]. That is, Ca^{2+} levels that are neither too high nor too low are suitable for biomechanical applications in tissue reconstruction. Thus, it is reasonable to postulate that preparing an appropriate cocktail of thrombin and Ca^{2+} is an efficient strategy to improve the biomechanics of PRP-based constructs.

Therefore, we recognized that the engineering constructs should reestablish not only the structural properties, such as those of the cell and matrix, but also the biochemical and biomechanical functions. To realize this aim, we designed a simple, three-step method to manufacture PRP-based engineering constructs with enzyme-ion-responsive biomechanical properties, appropriate biofactors, and favorable cell sources (Fig. 1). In brief, we employed CPCs as the favorable cell source, optimized platelet concentration for favorable growth factors, and strengthened PRP + CPC constructs using Ca^{2+} -thrombin cocktail. Considering the simultaneous optimizations of 3 basic elements of tissue engineering including cell resources, biochemistry, and biomechanics, we hypothesized that this orchestrated triple-optimized PRP + CPC construct could reconstruct cartilaginous microstructure and restore proper cartilage biomechanics both *in vitro* and *in vivo*.

2. Materials and methods

2.1. Isolation, expansion, and identification of CPCs

After obtaining institutional review board of People's Liberation Army General Hospital (CAAE: 14878813.4.0000.5533), fresh articular cartilages were obtained from the femur condyle of 5 road-accident patients undergoing lower limb amputation (3 males and 2 females, with an average age of 32 years). CPCs were obtained from non-weightbearing area of the lateral aspect of lateral femoral condyle and incubated as previously described in our published study [19]. Chondrogenic, osteogenic, and adipogenic inductions were performed to explore the multi-lineage differentiation ability of these CPCs, and cell migration/chemotaxis assays were performed to assess migratory capabilities according to a previous study [19].

2.2. Preparation of PRP

The blood samples were obtained from the five donors. A double centrifugation process was conducted to prepare PRP as previously described [29]. In brief, whole blood samples were centrifuged at 300g for 10 min before the whole upper phase and the top red layer (1–2 mm) were taken for a second centrifugation at 1200g for another 10 min. Then 85% volume of plasma was removed from the upper layer of centrifuge tube, and only 1–2 ml of plasma at the bottom of the centrifuge tube was reserved as PRP. The platelet concentration in the prepared PRP was determined using a cytoanalyzer. Per the measured platelet concentration, different volumes of plasma in the upper phase after second centrifugation were added to the prepared PRP to create a series of PRPs with concentrations of 500×10^9 platelets (pl)/L, 1000×10^9 pl/L, 2000×10^9 pl/L, 3000×10^9 pl/L, 4000×10^9 pl/L, and 5000×10^9 pl/L. Serum was considered PRP with 0×10^9 pl/L. Human TGF- β 1, PDGF-AB, IGF1, and bFGF concentrations in the series of PRPs were determined according to the reagent protocols of the quantitative Enzyme-linked Immunosorbent Assay (ELISA) Kits (R&D Systems, Minneapolis). Optical density was determined at 450 nm as previously

reported [16].

2.3. Optimization of platelet concentration for PRP constructs

Chondrogenic differentiation of CPCs cocultured with PRP were assessed to screen the optimal platelet concentration for preparing construct. Briefly, the aforementioned series of PRPs were activated with a cocktail of 10% CaCl_2 and bovine thrombin (20 U/mL) in 1:9 vol/vol to create PRP gels following a centrifugation at 3000g for 10 min to collect the supernatant, which was considered as activated PRPs. Then, third-generation CPCs were seeded at a density of 2000 cells per well in 48-well culture plates and the aforementioned activated PRPs were added to the reservoirs in 10% vol/vol. After 2 weeks of induction, CPCs were fixed in 4% paraformaldehyde and stained with antibodies for human collagen type I (Col-I), collagen type II (Col-II), collagen type X (Col-X) (BD Biosciences), and Sox-9 (R&D systems). The cell nuclei were stained with 40, 6-diamidino-2-phenylindole (DAPI) (Vector Laboratories). To analyze matrix formation of CPCs, Toluidine Blue, Safranin-O and Alcian Blue staining were carried out. The images were observed and captured by a fluorescence microscope (Olympus BX53). To evaluate gene expression levels of human Col-I, Col-II, Sox-9, and aggrecan in CPCs, RT-qPCR analysis (Table S1) was conducted.

2.4. Reinforcement of biomechanics for PRP constructs

To achieve the reinforced biomechanics of constructs, PRPs with 4000×10^9 pl/L were mixed with a series of cocktails of 5% CaCl_2 , 10% CaCl_2 , 15% CaCl_2 intersecting with 0 U/ml bovine thrombin (BT), 20 U/ml BT, 40 U/ml BT and 80 U/ml BT in 1:9 vol/vol. Tensile strength test, compression test, and shear test were carried out as previously described [19,30,31]. Additionally, considering that rheological property was another crucial mechanical characterization to investigate the PRP gel mechanics during the cross-linking process, oscillatory rheology of PRP was further conducted [32,33]. Briefly, each 5 ml PRP with concentration of 4000×10^9 pl/L was mixed with the aforementioned series of cocktails of CaCl_2 and BT to create PRP constructs in a culture dish with diameter of 2 cm. The following rheological experiments of the PRP constructs were performed using HAAKE Rheometer 600 with a parallel plate (20 mm diameter, 0.5 mm gap) in oscillatory mode at 37 °C with a certain oscillatory amplitude sweep ($\gamma = 0.1$ –100, $f = 1$ Hz) within the linear viscoelastic region. All the experiments were performed in three parallel samples.

2.5. Improvement of biodegradability for PRP constructs

To assess the biodegradability of PRP constructs, PRPs with 4000×10^9 pl/L were mixed with the aforementioned series of cocktails of CaCl_2 and BT. A trephine with a diameter of 5 mm (Nouvag AG) was used to mold PRP constructs with similar shapes. Then, these PRP gels were immersed in PBS at 37 °C (pH 7.4) following measurement of weight after removing the water on the surface every day. All the experiments were performed in three parallel samples.

To calculate the release of pro-inflammatory cytokines during hydrogel degradation, the released amount of IL-1 β and IL-6 were quantified using ELISA kits (R&D Systems, Minneapolis) on day 6. Optical density was determined at 450 nm.

2.6. Morphological characteristics of the triple-optimized PRP + CPC constructs

Flow cytometry analysis of platelet membrane markers, i.e., CD41a and CD42b, and transmission electron microscopy (TEM) for the observation of platelet ultrastructure were conducted to assess the purity and integrity of platelets in PRP constructs. Scanning electron microscopy (SEM) and HE staining (hematoxylin-eosin) were carried out to characterize the histological and ultrastructural morphologies of the

PRP + CPC constructs.

2.7. *In vitro* cartilage regeneration of constructs

To create PRP + CPC constructs, 1×10^6 CPCs at passage 3 were collected and suspended by 500 μ L of PRPs, followed by treatment of a cocktail of 10% CaCl_2 –40U/ml BT or not (Table 1). Constructs were cultured in DMEM supplemented with 10% vol/vol FBS, and incubated at 37 °C in an atmosphere of 5% CO_2 . For chondrogenic differentiation, 1×10^6 CPCs were centrifuged in polypropylene tubes at 300g for 10 min to form a pellet and maintained in chondrogenic induction medium consisting of DMEM, supplemented with 1% vol/vol insulin-transferrin-selenium, 10^{-7} M dexamethasone, 1 mM sodium pyruvate, 50 μ M ascorbate-2-phosphate, 50 μ g/mL proline, and 20 ng/mL TGF- β 3, which was regarded as a successful method to generate cartilage *in vitro* and can serve as positive control group according to previous studies [17,19,34]. On day 28, the constructs were fixed and sectioned, followed by evaluation of the cartilaginous matrix by HE, toluidine blue, and Safran-O staining. The expression of Col-II was detected by immunohistochemistry [35]. The images were captured using a microscope under brightfield mode and evaluated blindly by 5 graders according to the guidelines of the visual scoring system (Bern Score) based on published protocols for *in vitro* generated cartilaginous tissue [36]. For determining the biomechanical capacity of regenerated cartilage, the regenerated tissues from 6 groups were cut into square sections (2 mm³) along the long axis and subjected to biomechanical tests including tensile, compressive, and shear testing [19].

2.8. Implantation of the PRP + CPC constructs in the rabbit model

The animal experiment was approved by the Institutional Animal Care and Use Committee of PLA General Hospital. PRP + CPC constructs prepared from the five donors were molded by a trephine with a diameter of 5 mm (Nouvag AG) for implantation. A total of 30 5-month male New Zealand White rabbits were purchased from Beijing Vital River Laboratory Animal Technology Co., Ltd., and equally allocated into 6 groups as shown in Table 1. Under anesthetic with intramuscular injections of ketamine hydrochloride (60 mg/kg) and xylazine (6 mg/kg), the patella was dislocated to expose the distal femur, followed by the creation of a critical-sized cylindrical cartilage defects (5 mm in diameter and 2 mm in depth) on the femur trochlea by using the trephine [37]. Post debridement of the margins of the lesion, the PRP + CPC constructs were implanted into the defects and the patella was reset. After closing the capsule with sutures, the operated limb was immobilized for 7 days by splints to preserve primary healing.

At 12 weeks after the operation, the rabbits were sacrificed, and the operated distal femurs were dissected followed by macroscopic observation, histological analysis, and biomechanical examination. Briefly, histological examination and immunohistochemistry were performed for general histology. Alcian blue, Safranin-O, Toluidine blue staining,

and immunohistochemical analysis were performed to assess the cartilaginous matrix distribution. The International Cartilage Repair Society (ICRS) assessment scores for cartilage repair all samples were used to grade the regenerated tissue [38]. To evaluate the cartilaginous matrix formation *in vivo*, human Col-I, Col-II, Sox-9, and aggrecan gene expression levels of newborn tissues were analyzed by RT-qPCR. For determining the biomechanical capacity of regenerated cartilage, the newborn tissues from 6 groups were cut into square sections (2 mm³) along the long axis and subjected to tensile, compressive, and shear testing [19].

2.9. Statistical analysis

At least triplicate parallel samples were performed for each set of results. The outcomes were assumed to have a normal distribution and homogeneous variance. One-way analysis of variance (ANOVA) and Bonferroni post hoc tests using SPSS 18.0 software (SPSS, Inc., Chicago, IL, USA) was used to analyze the differences among the groups. The data are expressed as the mean \pm standard error of the mean (SEM). A *P* value of less than 0.05 was considered statistically significant (**P* < 0.05, ***P* < 0.01, and ****P* < 0.001).

3. Results

3.1. Identification and characteristics of CPCs

Approximately 2 weeks after the initial culture, primary CPCs were expanded in a monolayer and exhibited a fibroblast-like morphology. When the cells were transferred after 2–5 generations, they had homogeneously long fusiform or polygonal structures (Fig. S1A). Compared with chondrocytes, CPCs responded much more strongly to treatment with HMGB1, at a level approximately 2.0- to 2.5-fold that of the control groups, indicating its prominent migratory capacity (Fig. S1B). Additionally, strong positive Alcian blue and Toluidine blue staining in the chondroinductive CPCs revealed their intrinsic propensity for chondrogenesis. Furthermore, intracellular ALP and mineralized matrix could be observed in the osteoinductive CPCs, but intracytoplasmic lipid droplet accumulation was only slightly visible in the adipogenic-inductive CPCs, indicating their maintained potential to become osteocytes but limited fate toward adipocytes (Fig. S1C). The mRNA expression levels of Col-II, Sox-9, OCN, Runx-2, CEBP/ α , and PPAP/ γ in CPCs after treatment with the trilineage induction medium further conformed their intrinsic propensity toward chondrogenesis (Fig. S1D). These results substantially support CPCs as a favorable cell source in PRP-based cartilage tissue engineering, which can undergo multilineage differentiation but its lineage is restricted to differentiate into chondrocytes.

3.2. Optimization of biochemical properties for PRP constructs

To evaluate the potential impacts on the chondrogenic capability of

Table 1
Experimental groups of the *in vitro* and *in vivo* studies.

	Groups	Optimization	Treatment
<i>In vitro</i>	CPC group	Control	Pellets of 1×10^6 CPCs post centrifugation
	PRP + CPC group	Single	PRP with 1070×10^9 pl/L + CPC constructs
	Biochemical PRP + CPC group	Dual	PRP with 4000×10^9 pl/L + CPC constructs
	Biomechanical PRP + CPC group	Dual	PRP with 1070×10^9 pl/L treated with cocktail of 10% CaCl_2 –40U/ml BT + CPC constructs
	Triple-optimization group	Triple	PRP with 4000×10^9 pl/L treated by cocktail of 10% CaCl_2 –40U/ml BT + CPC constructs
	Chondrogenic-induction group	Positive control	Chondrogenic-induced CPC constructs
<i>In vivo</i>	Untreated group	Non	Cartilage defects without treatment
	PRP + CPC group	Single	PRP with 1070×10^9 pl/L + CPC constructs
	Biochemical PRP + CPC group	Dual	PRP with 4000×10^9 pl/L + CPC constructs
	Biomechanical PRP + CPC group	Dual	PRP with 1070×10^9 pl/L treated with cocktail of 10% CaCl_2 –40U/ml BT + CPC constructs
	Triple-optimization group	Triple	PRP with 4000×10^9 pl/L treated by cocktail of 10% CaCl_2 –40U/ml BT + CPC constructs
	Positive control group	Native	Sham-operated

PRP, platelet-rich plasma; CPC, chondrogenic progenitor cells; BT, bovine thrombin.

CPCs induced by PRPs with different platelet concentrations, cellular immunofluorescence, cytochemical staining, and qPCR analysis were performed. Results in Fig. 2A show the discriminatory chondrogenic-related protein expression along with the treatments of a series of PRPs: gradually increased Sox-9 and Col-II components were detected when the PRP concentrations were below 4000×10^9 pl/L, whereas

gradually decreased Col-I and Col-X contents were detected when the PRP concentrations were below 5000×10^9 pl/L; meanwhile, these contents were comparable to each other between the 3000×10^9 pl/L and 4000×10^9 pl/L groups. These data suggest that the most effective CPC chondrogenesis stimulated by PRP requires a platelet concentration within a certain range; this range might be within 3000×10^9 pl/L to

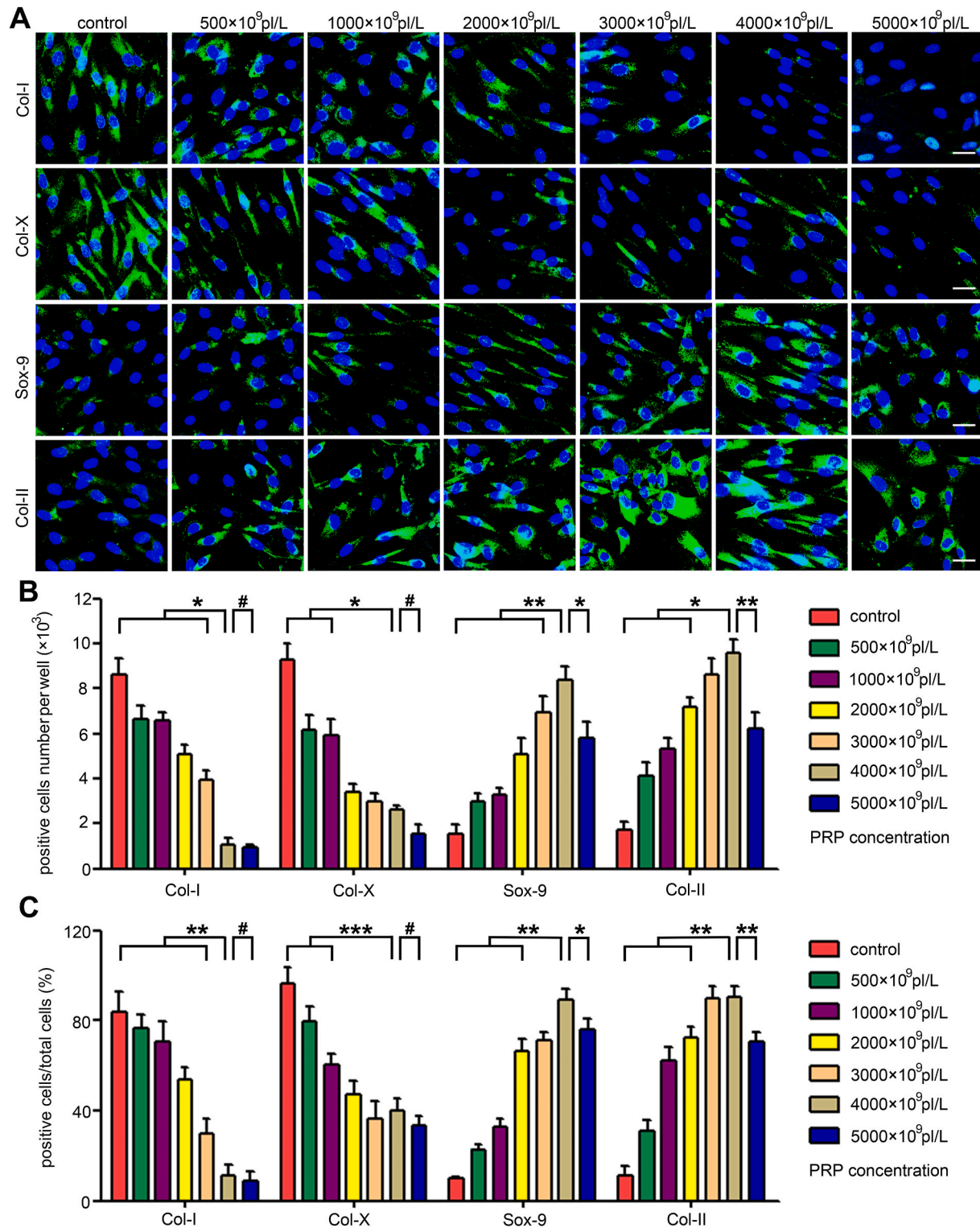


Fig. 2. Optimization of platelet concentration for CPC chondrogenesis. (A) Immunofluorescence analysis of the secretion of Col-I, Col-II, Col-X, and Sox-9 in CPCs exposed to different concentrations of PRP. Scale bars represent 10 μ m. (B) Col-I, Col-II, Col-X, and Sox-9 positive cell ratios after the PRP stimulation. (C) Col-I, Col-II, Col-X and Sox-9 positive cell numbers after the PRP treatment. Data are presented as mean \pm SEM, $n = 3$, * $P < 0.05$, ** $P < 0.01$, *** $P < 0.001$ and # $P > 0.05$.

4000×10^9 pl/L. Quantitative analyses of the positive cell number (Fig. 2B) and positive cell ratio (Fig. 2C) further confirmed that the optimized PRP concentration for CPC chondrogenesis should be 3000×10^9 pl/L~ 4000×10^9 pl/L.

To further validate the optimized concentrations of PRP on CPC chondrogenesis, chondrogenic-specific cytochemical staining was carried out. As shown in Figs. S2A and a similar trend was detected in the Alcian blue-, Safranin-O- and Toluidine blue-stained areas across the series of PRP-treated groups as that detected in the immunofluorescence analyses. Positive cell numbers and cell ratios further illustrated the superiority of PRP concentrations of 3000×10^9 pl/L~ 4000×10^9 pl/L for CPC chondrogenesis, resembling the results of cellular immunofluorescence and cytochemical staining (Figs. S2B and S2C). Furthermore, qPCR analysis revealed that there were increasing Sox-9, Col-II, and aggrecan expression levels and decreasing Col-I expression level along with the elevation of platelet concentration (Figs. S3A–D). Although the 4000×10^9 pl/L group exhibited the highest expression levels of Col-II, Sox-9, and aggrecan, there was no significant difference between the 3000×10^9 pl/L and 4000×10^9 pl/L groups. Considering that PRP with

a platelet concentration of 4000×10^9 pl/L exhibited higher efficacy than that with 3000×10^9 pl/L in some conditions, we ultimately selected 4000×10^9 pl/L as the optimal platelet concentration for PRP + CPC constructs.

3.3. Reinforcement of biomechanical properties for PRP constructs

To reinforce the PRP construct strength, a series of cocktails of CaCl_2 and thrombin were added into PRPs following mechanical detection. As shown in Fig. 3A–C, oscillatory rheological analysis demonstrated larger G' than G'' with prolonged strain in all kinds of PRP gels, illustrating that the elastic component of the gel dominates the viscous component. Meanwhile, it was found that whether in 5% CaCl_2 , 10% CaCl_2 , or 15% CaCl_2 groups, 40 U/ml BT-treated PRP gels exerted greater values of G' than other BT-treated gels, and that the G' of 40 U/ml BT-treated gels in the 10% CaCl_2 group was significantly higher than that of their counterparts in the 5% CaCl_2 and 15% CaCl_2 groups. Furthermore, the crossover point in the 10% CaCl_2 group (strain = 42) was later than those in the 5% (strain = 18) and 15% (strain = 38) groups (Fig. 3A–C).

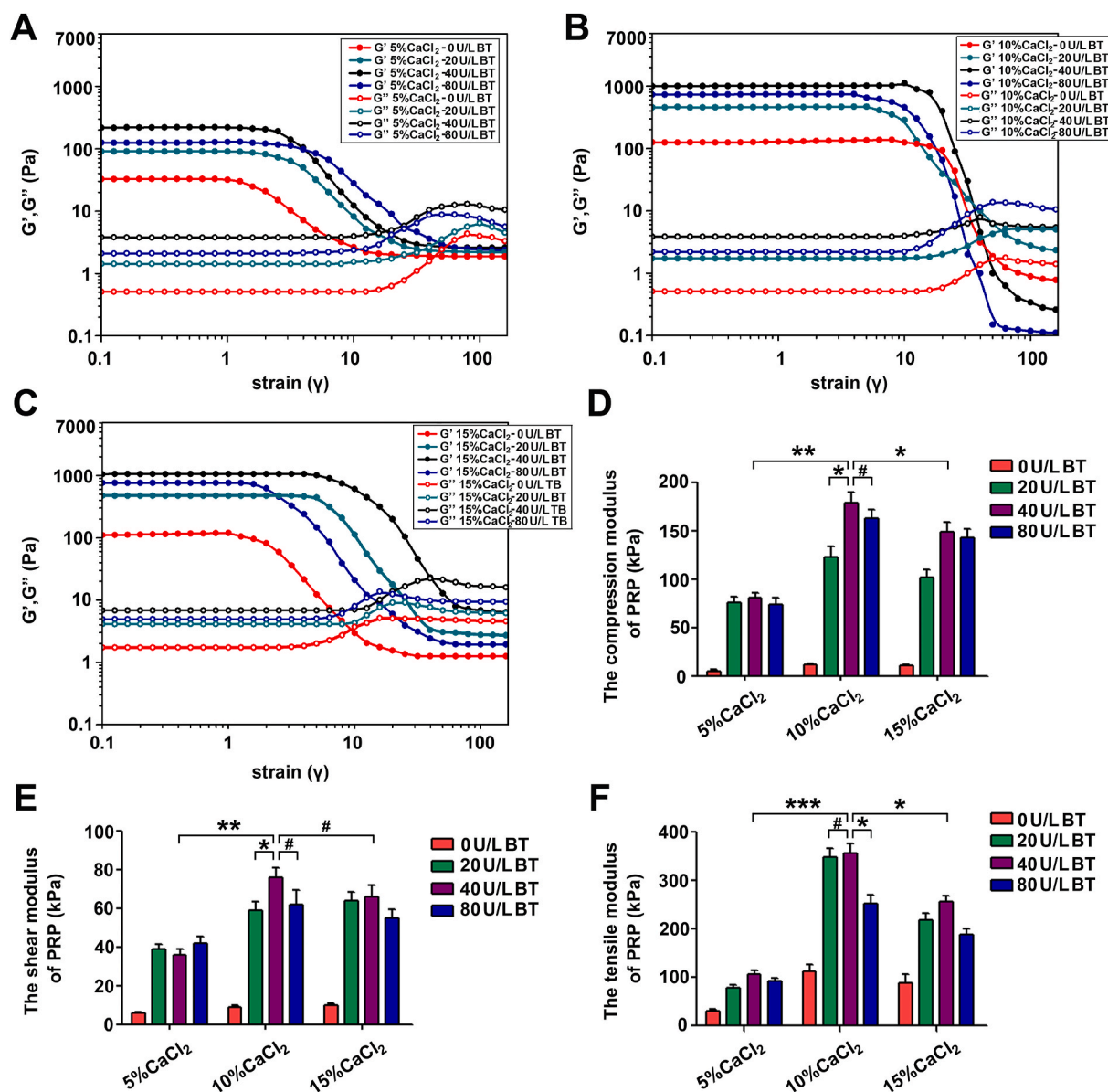


Fig. 3. Reinforcement of biomechanical properties for PRP constructs. (A–C) Rheological properties of CaCl_2 -bovine thrombin (BT) cross-linked PRP gels. (D–F) Compressive, shear and tensile tests of CaCl_2 -BT cross-linked PRP gels. Data are presented as mean \pm SEM, $n = 3$, * $p < 0.05$, ** $p < 0.01$, *** $p < 0.001$ and # $p > 0.05$.

Compression testing, shear testing, and tensile strength testing were further carried out to evaluate the PRP gel biomechanics. As shown in Fig. 3D, when the thrombin concentration was set at 40 U/ml, the compressive modulus of the constructs increased from 80.8 ± 5.1 to 178.8 ± 11.1 kPa as the CaCl_2 concentration increased from 5% to 10%. However, when the CaCl_2 concentration increased to 15%, the compressive modulus was observed to decrease but did not significantly differ from the 10% compressive modulus (148.8 ± 10.1 kPa, $P > 0.05$). The shear and tensile testing showed similar trends among the 5%, 10%, and 15% experimental groups (Fig. 3E–F). These results suggest that the Ca^{2+} -thrombin-assisted networks remarkably improved the mechanical properties of PRP gels; nevertheless, when Ca^{2+} concentration is beyond 10% or thrombin concentration exceeds 40 U/ml, the efficacy is tarnished. Therefore, 10% CaCl_2 -40 U/ml BT was ultimately employed to improve PRP gel mechanical properties.

3.4. Improvement of biodegradability for PRP constructs and detection of pro-inflammatory cytokines

Biodegradability is an important property of scaffolds, which can affect the regenerative process of tissues especially the formation of primary regenerated tissue and the following remodeling [33]. To further characterize the gel properties, we investigated the biodegradability of

gels prepared by activating platelet with thrombin and CaCl_2 . PRPs with 4000×10^9 pl/L were mixed with a series of cocktails of 5% CaCl_2 , 10% CaCl_2 , 15% CaCl_2 intersecting with 0 U/ml bovine thrombin (BT), 20 U/ml BT, 40 U/ml BT and 80 U/ml BT in 1:9 vol/vol. As shown in Fig. 4A–F, when the concentration of BT was set at 5% CaCl_2 , the weights of PRP gels in 80 U/ml and 40 U/ml were parallel to each other and significantly higher than those in 20 U/ml and 0 U/ml groups. Results in the 10% CaCl_2 and 15% CaCl_2 showed similar trends. On the other side, we found that the weight of residual gels increased gradually with the elevation of CaCl_2 concentration, and that there was no remarkable differences in these values between groups 10% CaCl_2 and 15% CaCl_2 . These results suggest that the Ca^{2+} -thrombin-assisted networks effectively improve the biodegradability of PRP gels; nevertheless, when Ca^{2+} concentration is beyond 10% or thrombin concentration exceeds 40 U/ml, the efficacy is abolished. Therefore, PRP gel treated with 10% CaCl_2 -40 U/ml BT can be selected as the ideal scaffold, even from the perspective of biodegradation.

Additionally, concentration of pro-inflammatory cytokines (IL-1 β , IL-6) was determined using ELISA kits. As shown in Fig. S4A, with the increase of CaCl_2 concentration, there was a similar level in the concentration of IL1 β within the three kinds of preparations (5% CaCl_2 groups, 10% CaCl_2 groups, and 15% CaCl_2 groups). Meanwhile, it was observed that whether in 5% CaCl_2 , 10% CaCl_2 , or 15% CaCl_2 groups, 40

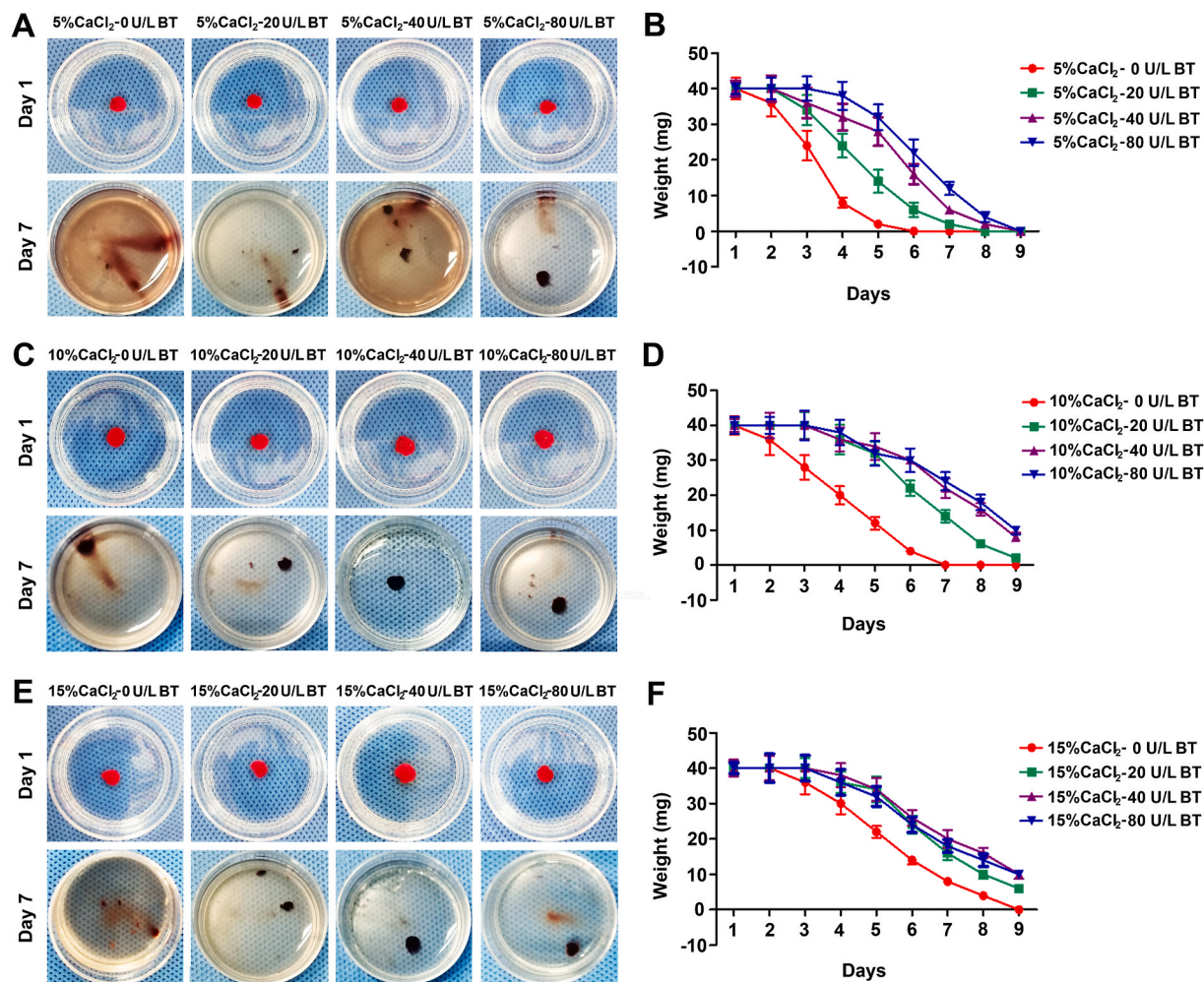


Fig. 4. The degradation properties of PRP gels. (A–B) The weights of PRP gels treated with cocktails of 5% CaCl_2 combined with 0 U/ml bovine thrombin (BT), 20 U/ml BT, 40 U/ml BT, or 80 U/ml BT in 1:9 vol/vol, after being immersed in PBS at 37 °C for 1, 2, 3, 4, 5, 6, 7, 8, and 9 days. (C–D) The weights of PRP gels treated with cocktails of 10% CaCl_2 combined with 0 U/ml BT, 20 U/ml BT, 40 U/ml BT, or 80 U/ml BT in 1:9 vol/vol, after immersion in PBS at 37 °C on day 1, 2, 3, 4, 5, 6, 7, 8, and 9. (E–F) The weights of PRP gels treated with cocktails of 15% CaCl_2 combined with 0 U/ml BT, 20 U/ml BT, 40 U/ml BT, or 80 U/ml BT in 1:9 vol/vol, after being immersed in PBS at 37 °C for 1, 2, 3, 4, 5, 6, 7, 8, and 9 days. Data are presented as mean \pm SEM, $n = 3$, * $P < 0.05$ and # $P > 0.05$.

U/ml BT-treated PRP gels possessed similar values of IL1 β concentration to other BT-treated gels. Similarly, for IL-6, there were no significant differences among these preparations (Fig. S4B).

3.5. Morphological, structural and biochemical analyses of the optimized PRP + CPC constructs

To better understand the newly developed constructs, flow cytometry analysis, HE staining and SEM were carried out. As indicated in Fig. 5A–E, the achieved PRP comprised large amounts of platelets with the CD41a and CD42b double-positive cell ratio of $92.14 \pm 0.66\%$, highlighting the successful preparation of PRP within integrated and functional platelets. After activation by a cocktail of 10% CaCl₂-40 U/ml BT, light red and semitransparent PRP gels were created (Fig. 5F). HE staining revealed a uniformly distributed crosslinked fibrin network and subsequently formed meshes in the stained sections (Fig. 5G–H). Additionally, as shown in Fig. 5L–M, abundant mononuclear cells shown in dark blue were randomly encapsulated into the skeleton and stretched in the network, demonstrating the feasibility for CPCs to survive and proliferate in a 3-D microstructure. SEM images of the samples revealed that the strongly crosslinked fibrin skeleton consolidated a micrometer-scale mesh-like microstructure in the optimized PRP + CPC constructs (Fig. 5I–J), allowing CPCs to adhere to the fiber skeleton and extend into the 3-D microstructure (Fig. 5N–O). Finally, concentrations of growth factors in the construct were determined using ELISA: TGF β 1 (231.21 ± 22.65 ng/ml), bFGF (2.67 ± 0.43 ng/ml), IGF1 (166.21 ± 22.46 ng/ml), and PDGF-AB (204.73 ± 19.63 ng/ml).

3.6. Cartilage regeneration of the optimized PRP + CPC constructs *in vitro*

To determine the efficacy of the optimized PRP + CPC constructs to reconstruct cartilage, CPC constructs, PRP + CPC constructs with single-, dual- or triple-optimizations were cultured *in vitro* for 28 days (Table 1). PRP at a concentration of 1070×10^9 pl/L was randomly chosen as the unoptimized PRP, which was within the range of PRP concentration commonly used in clinical trials or laboratory investigations [39]. As indicated in Fig. 6A and E, the results of HE staining in the group with triple-optimization showed a significantly larger area of cartilage-like tissue (the average cross area of regenerated tissues was 0.39 cm²) than those in the sole CPC (0.18 cm², $P < 0.001$) and single- (0.24 cm², $P < 0.01$) or dual- (0.27 cm², $P < 0.05$) optimized PRP + CPC groups but was comparable to that in the chondrogenic induction group (0.41 cm², $P > 0.05$). To further evaluate cartilage regeneration, the secretion of the cartilaginous matrix, such as proteoglycans and glycosaminoglycans, was detected using histochemical staining. The data of Safranin-O and Toluidine blue staining consistently showed increased positive staining areas as more elements were optimized; tissue in the triple-optimization groups exhibited a predominant positive zone, similar to chondrogenic-induced cartilage (Fig. 6B and C). Immunohistochemistry of Col-II further showed that the seeded CPCs in triple-optimization groups possessed a remarkably greater possibility of differentiating into a chondrocyte-like cell phenotype compared with those in single- or dual-optimization groups (Fig. 6D). Quantitatively, the pellet scores were 2.62 in the control group, 5.19 in the PRP + CPC group, 6.71 in the biochemical PRP + CPC group, 6.14 in the biomechanical PRP + CPC group, 8.66 in the triple-optimization group, and 9.23 in the sham group. The triple-optimization group exhibited

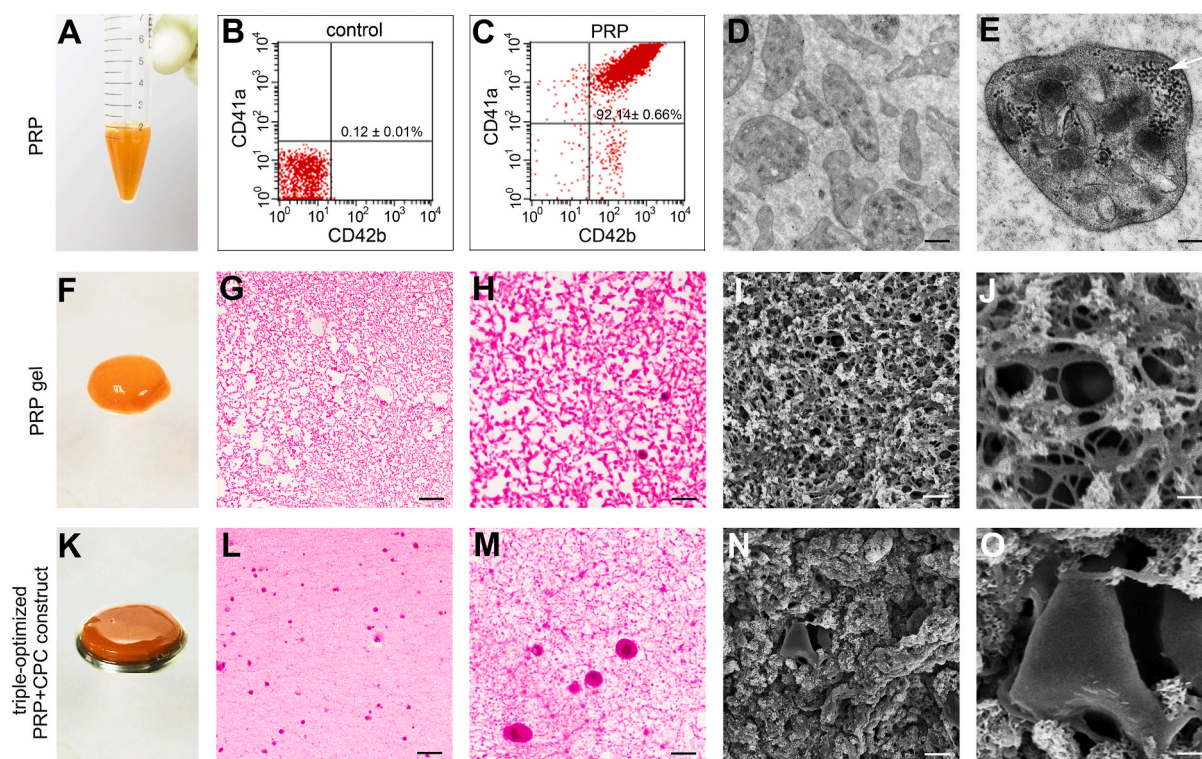


Fig. 5. Morphological characteristics of the triple-optimized PRP + CPC construct. (A) Gross observation of PRP with 4000×10^9 pl/L (B, C) Flow cytometry analysis of platelet membrane markers, i.e., CD41a and CD42b. (D, E) Ultrastructure of platelets presented by the TEM analysis. Scale bars in graphs (D) and (E) are $4 \mu\text{m}$ and $1 \mu\text{m}$, respectively. The white arrow indicates α -particles in platelets. (F) Gross appearance of the PRP gel. (G, H) Histological morphology of the PRP gel. Scale bars represent $200 \mu\text{m}$ and $50 \mu\text{m}$ in graphs (G) and (H), respectively. (I, J) Ultrastructure of the PRP gel. Scale bars in graphs (I) and (J) are $100 \mu\text{m}$ and $40 \mu\text{m}$, respectively. (K) Gross observation of the triple-optimized PRP + CPC construct. (L, M) Histological morphology of the triple-optimized PRP + CPC construct. Scale bars in graphs (L) and (M) are $100 \mu\text{m}$ and $25 \mu\text{m}$. (N, O) Ultrastructure of the triple-optimized PRP + CPC construct. Scale bars in graphs (N) and (O) are $10 \mu\text{m}$ and $2 \mu\text{m}$.

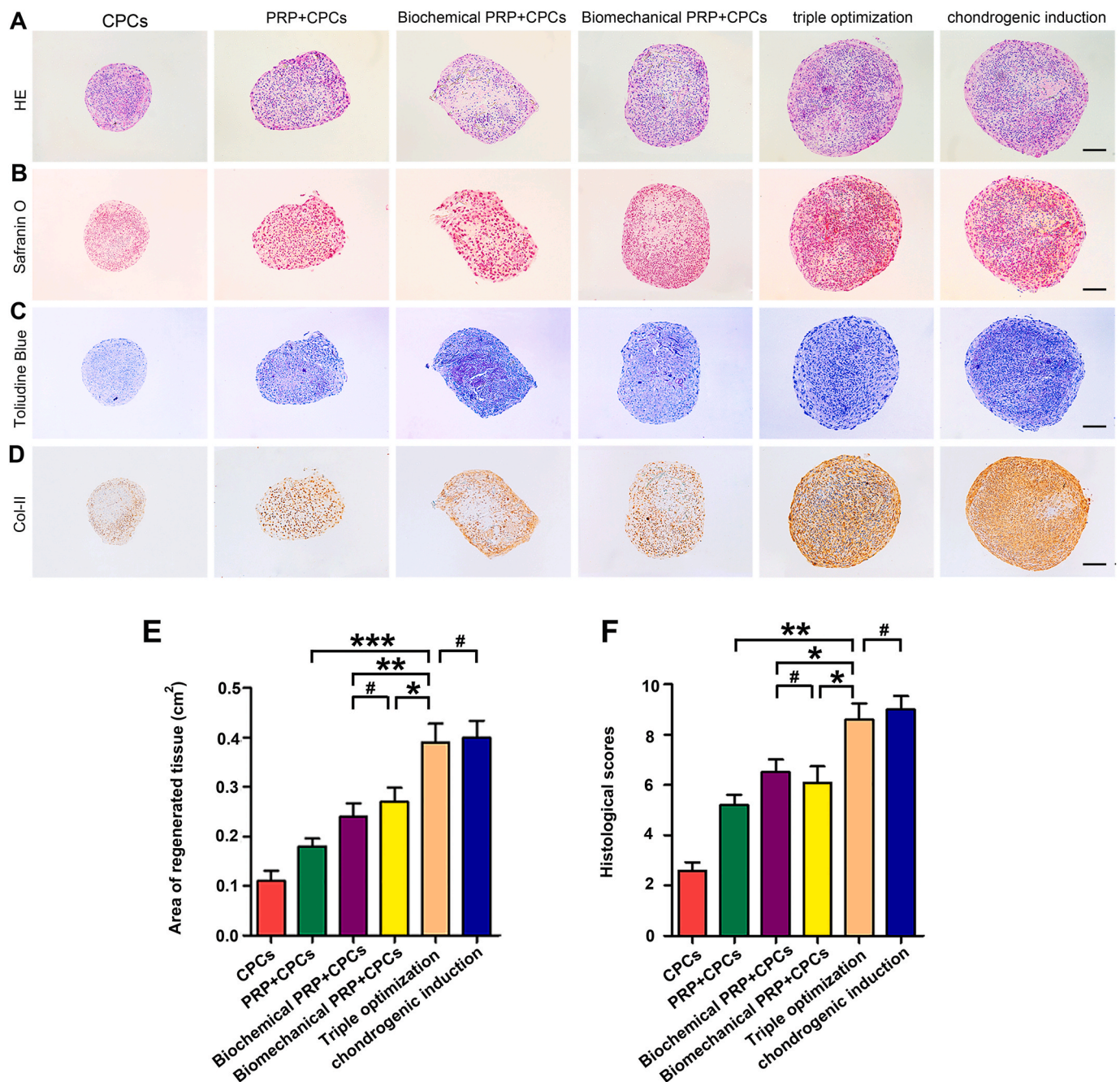


Fig. 6. Cartilage regeneration of the optimized PRP + CPC constructs after 4-week cultivation *in vitro*. (A) HE staining of CPC construct, PRP + CPC construct, biochemical PRP + CPC construct, biomechanical PRP + CPC construct, triple-optimized construct, and chondrogenic induction construct post-28-day cultivation *in vitro*. The chondrogenic induction group was considered a positive control. Scale bars = 1 mm. (B–D) Representative sections stained with Toluidine Blue, Safranin-O, and Alcian Blue staining in the 6 groups at 4 weeks. Scale bars = 1 mm. (E, F) Measurement of the regenerated tissue area and evaluation of the histological scores based on the visual scoring system (Bern Score). Data are presented as mean \pm SEM, $n = 3$, * $P < 0.05$, ** $P < 0.01$, *** $P < 0.001$ and # $P > 0.05$. (For interpretation of the references to color in this figure legend, the reader is referred to the Web version of this article.)

significantly higher scores than the other 4 experimental groups ($P < 0.001$, $P < 0.01$, $P < 0.05$, and $P < 0.05$, respectively) but exhibited discernible differences compared with the sham group ($P > 0.05$) (Fig. 6F).

Moreover, qPCR analysis was performed to detect the expression profile of chondrogenic-related genes, including Col-I, Col-II, Sox-9, and aggrecan. As shown in Fig. 7A–D, remarkably lower expression levels of Col-I and significantly greater expression levels of Sox-9, Col-II, and aggrecan were observed in the triple-optimization group than in the single- or dual-optimization groups. Moreover, whether for Col-I, Sox-9, Col-II, or aggrecan genes, the mRNA expression levels in the triple-

optimization group did not significantly differ from those of the chondrogenic-induction group.

To detect the biomechanical properties of regenerated tissue, compression testing, shear testing, and tensile strength testing were performed. After culturing *in vitro* for 4 weeks, tissue in the triple-optimization group showed a higher compression modulus and a greater tensile modulus than that in the single- and dual-optimization groups but did not significantly differ from that in the chondrogenic-induction group (Fig. 7E and G). Nevertheless, regenerated tissue in the dual-optimization group possessed greater compression and tensile modulus values compared with those of the control and single-

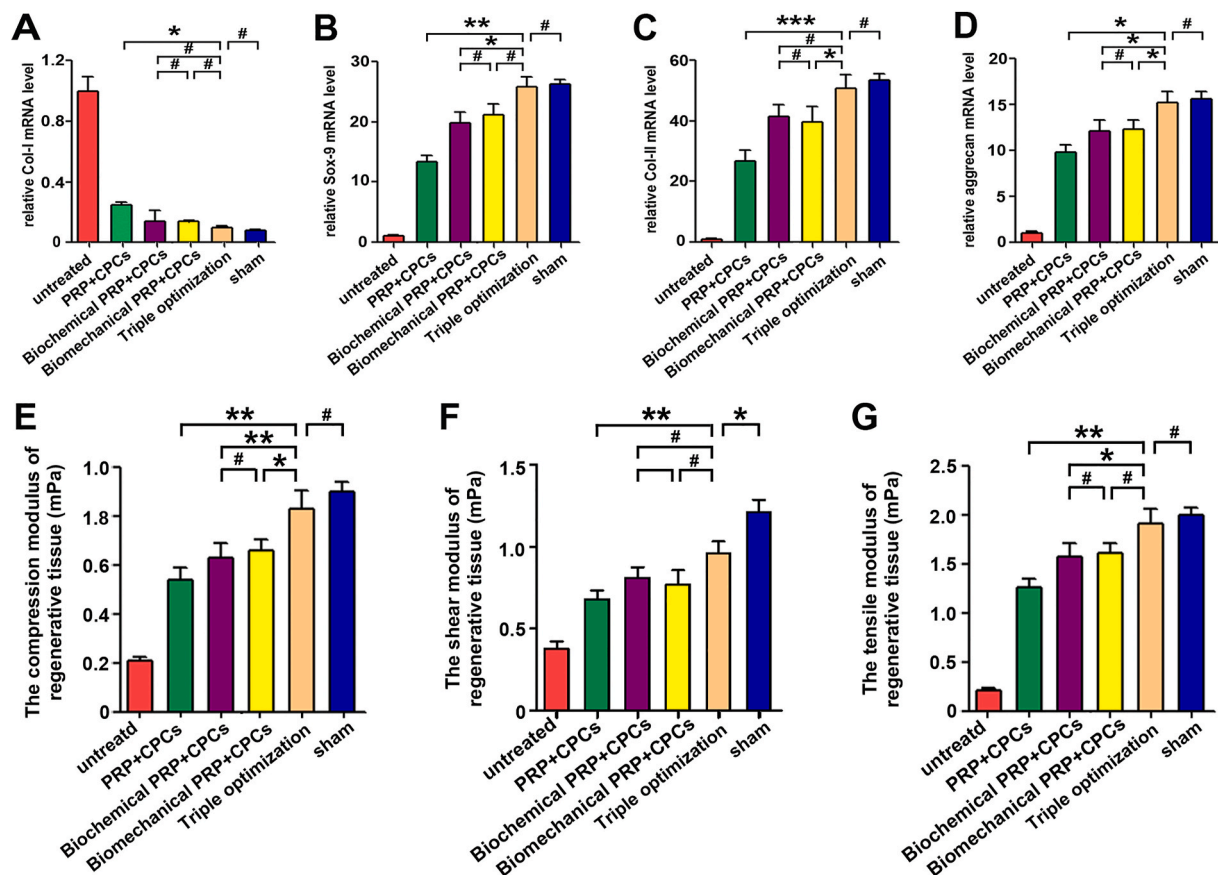


Fig. 7. Gene expression and biomechanical properties of the regenerated tissues after 4 weeks *in vitro*. (A–D) Relative expression levels of fibrogenic-related gene (Col-I) and chondrogenic-related genes (Sox-9, Col-II, and aggrecan) in engineered tissue after 4 weeks of *in vitro* culture. (E–G) Biomechanical properties of the *in vitro* constructs, including compressive modulus, shear modulus, and tensile modulus after 4 weeks of culture. Data are presented as mean \pm SEM, $n = 3$, $*P < 0.05$, $**P < 0.01$, $***P < 0.001$ and $^{\#}P > 0.05$.

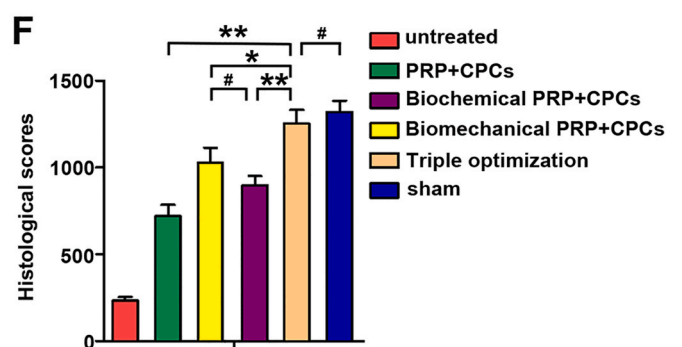
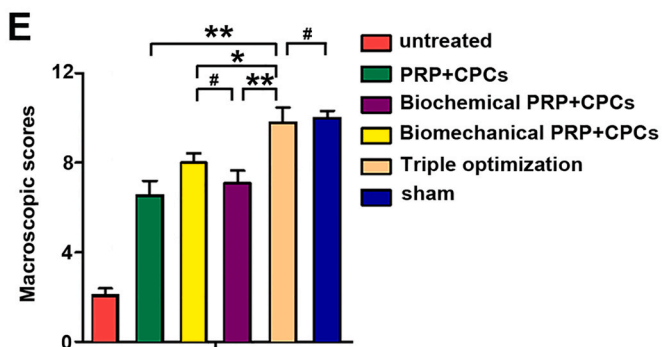
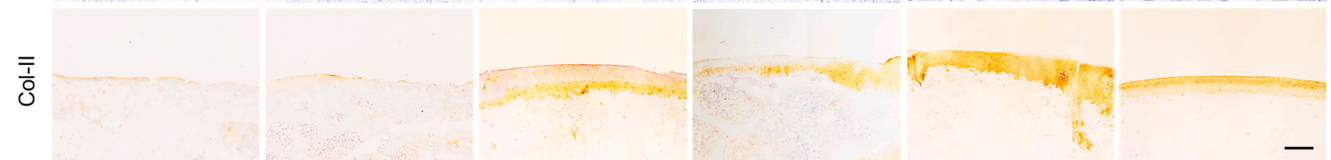
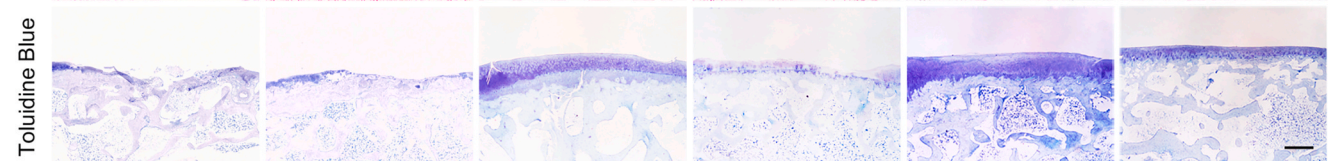
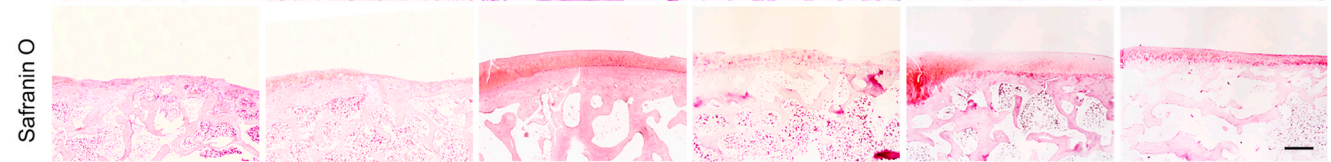
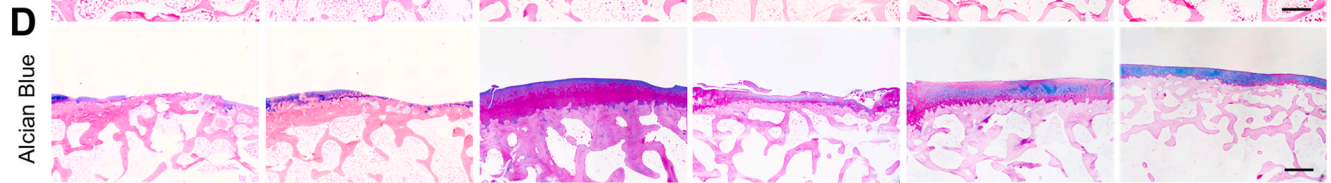
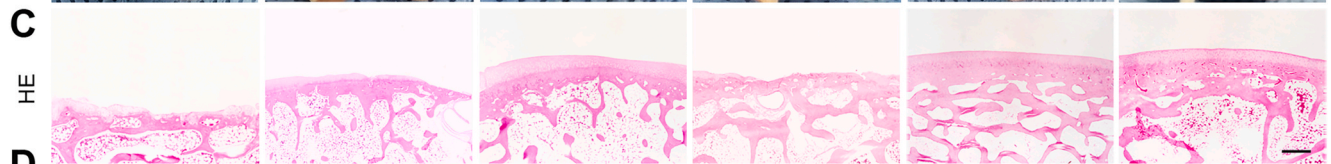
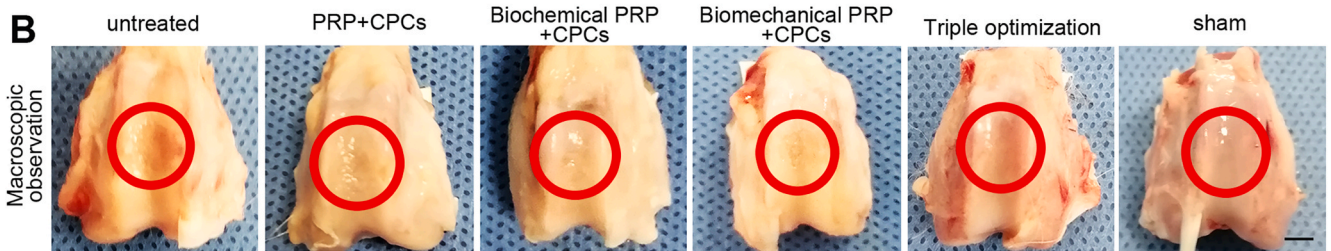
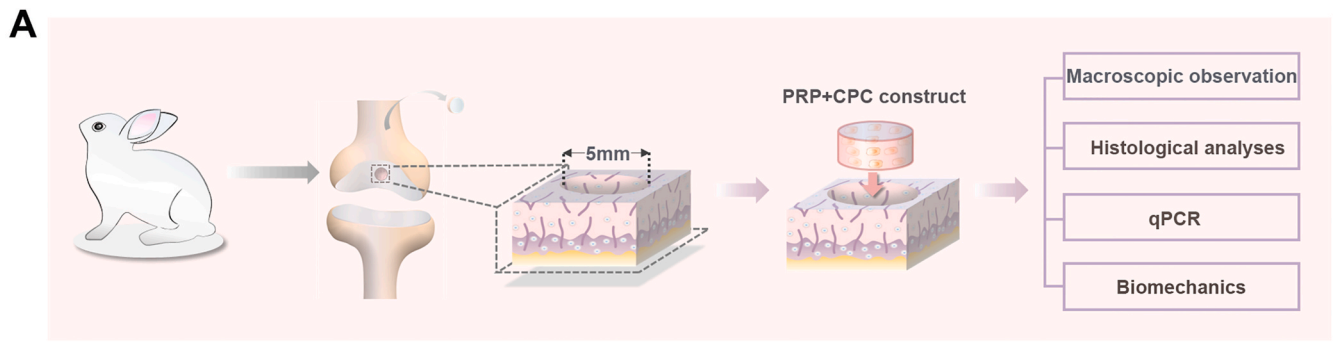
optimization groups. Besides, the shear testing showed significant differences among the single-, dual- and triple-optimization groups, as the shear modulus measured in the triple-optimization group possessed the greatest values, which were similar to those of the chondrogenic-induction group (Fig. 7F). These data suggested that tissues in the triple-optimization group consistently outperformed those in the single- and dual-optimization groups in biomechanical properties. Taken together, these findings demonstrated the superiority of triple-optimized PRP + CPC constructs for cartilage regeneration over single- and dual-optimization PRP + CPC constructs.

3.7. Cartilage regeneration of the optimized PRP + CPC constructs *in vivo*

The efficacy of *in vivo* cartilage regeneration was evaluated by implanting constructs into the knee joints of rabbits (Table 1). Macroscopic observation, histological analysis, qPCR, and biomechanical tests were carried out for further assessment (Fig. 8A). As shown in Fig. 8B, at 12 weeks after transplantation, the representative macroscopic observations displayed discriminatory regenerated tissue among the 6 groups. The surfaces of the tissues in the untreated group, PRP + CPC, biochemical PRP + CPC, and biomechanical PRP + CPC groups were less smooth than those in the triple-optimization group, which possessed a normal gross appearance with a shiny white color and integrated with the surrounding normal cartilage, resembling the normal cartilage. Although the regenerated tissue almost fully filled in the defects in all of the optimization groups, concavity, or fissures in some of the regenerated tissue could still be observed in the single- and dual-optimization groups, which was seldom seen in the triple-optimization group. Further quantitative assessment based on the ICRS scoring system

showed that the mean scores in the untreated, PRP + CPC, biochemical PRP + CPC, and biomechanical PRP + CPC groups were 2.11 ± 0.67 , 6.56 ± 0.63 , 8.07 ± 0.42 , and 7.10 ± 0.55 , respectively, which were significantly less than those in triple-optimization group (9.79 ± 0.66) (Fig. 8E).

To further compare different kinds of constructs in repairing cartilage defects in rabbits, HE staining, cytochemical staining, and immunohistochemistry were performed. HE staining in the untreated group showed that the defects were seldom filled with regenerated tissue, and only minimal fibrous tissue was observed on the bottom and in the periphery (Fig. 8C). The Alcian blue, Safranin-O, and Toluidine blue staining as well as the immunohistochemistry of Col-II also showed minimal positive staining areas in the untreated group (Fig. 8D). As the PRP + CPC construct was applied, HE staining revealed a much larger regenerated tissue area than that in the untreated group. However, the histochemical staining of the newly regenerated tissue was less than completely positive, indicating the unsatisfactory regeneration of cartilage. When biochemical optimization was carried out, the defects were completely filled with cartilage-like tissue. However, the content of the cartilaginous matrix was still less abundant than that of the normal cartilage. Moreover, the efficacy of the biochemical PRP + CPC was heterogeneous, and some samples still showed concavity or fissures in the defects. As biomechanical optimization was applied in the constructs, regenerated tissue was thinner compared with the surrounding normal cartilage, and the histochemical staining revealed that cartilage matrix formation mainly distributed in the peripheral area and the bottom. However, when the optimized cell source, appropriate biochemistry, and reinforced biomechanics were simultaneously applied in the implants, completely filled, regenerated tissue was



(caption on next page)

Fig. 8. Cartilage regeneration of the optimized PRP + CPC constructs after 12 weeks *in vivo*. (A) Schematic diagram of the *in vivo* procedure and the following assessment strategy. (B) Macroscopic observation of cartilage defect healing in the 6 groups post 12-week implantation. Scale bars = 2 mm. (C, D) Histological analyses of regenerated tissue in the 6 groups at 12 weeks post-implantation. Scale bars = 1 mm. (E, F) Macroscopic and histological quantitative assessments at 12 weeks after the operation, scored according to the International Cartilage Repair Society (ICRS). Data are presented as mean \pm SEM, $n = 5$, $*P < 0.05$, $**P < 0.01$ and $\#P > 0.05$.

consistently visible in the defects, and the histochemical staining showed a positive area dominating newly generated tissue, resembling the native cartilage (Figs. 8C and 6D).

Quantitative analysis was also performed based on the ICRS scoring system. As shown in Fig. 8F, the average scores were 233.3 ± 20.7 in the untreated group, 721.7 ± 63.3 in the PRP + CPC group, 1029.5 ± 87.6 in the biochemical PRP + CPC group, 897.4 ± 55.3 in the biomechanical PRP + CPC group, and 1254.3 ± 78.6 in the triple-optimization group. The triple-optimization group exhibited significantly higher scores than the single- and dual-optimization groups ($P < 0.01$, $P < 0.05$, $P < 0.01$, respectively).

For thoroughly determining the repair efficiency of the cartilage defects, the mRNA expression levels of chondrogenic-related genes in the regenerated tissue were analyzed by qPCR. The triple-optimization group exhibited significantly higher Sox-9, Col-II, and aggrecan expression levels but lower Col-I expression levels (25.9 ± 1.59 , 50.7 ± 4.55 , 15.4 ± 1.23 , and 0.12 ± 0.01 , respectively) than the PRP + CPC group (13.4 ± 0.97 , $P < 0.01$; 26.8 ± 3.51 , $P < 0.001$; 9.8 ± 0.79 , $P < 0.05$; and 0.25 ± 0.015 , $P < 0.05$, respectively), biochemical PRP + CPC group (19.8 ± 1.83 , $P < 0.05$; 41.7 ± 3.91 , $P > 0.05$; 12.4 ± 1.22 , $P < 0.05$; and 0.14 ± 0.07 , $P > 0.05$, respectively), and biomechanical PRP + CPC group (21.6 ± 1.78 , $P > 0.05$; 39.6 ± 5.02 , $P < 0.05$; 12.3 ± 0.97 , $P < 0.05$; and 0.15 ± 0.01 , $P > 0.05$, respectively) (Fig. 9A–D).

For assessing the efficacy of triple-optimized PRP + CPC construct for biomechanical recovery, biomechanical tests were performed. Although the shear moduli in both the single-, dual-, and triple-optimization groups were lower than that in the native group, the triple-optimization group consistently outperformed the single- and dual-optimization groups in shear testing (Fig. 9F). The compression and tensile moduli in the triple-optimization group consistently showed negligible differences compared with those of the native group, reaching the highest values among all 5 experimental groups (Fig. 9E and G). These results revealed that neither single- or dual-optimization can fully restore the cartilage characteristics of regeneration tissue and that only the triple-optimization treatment can satisfactorily enable cartilage regeneration with structural reconstruction and functional recovery on par with those of the native cartilage.

4. Discussion

Tissue engineering is an emerging therapeutic method that combines biomaterials, cells, and biological factors to develop biological substitutes that can notably restore the functions of alterations [40,41]. As one of the basic components, cell sources are the main population and the managers of regenerated tissue, thus playing a core role in engineering constructs [8,9]. Previous study compared CPC potential with

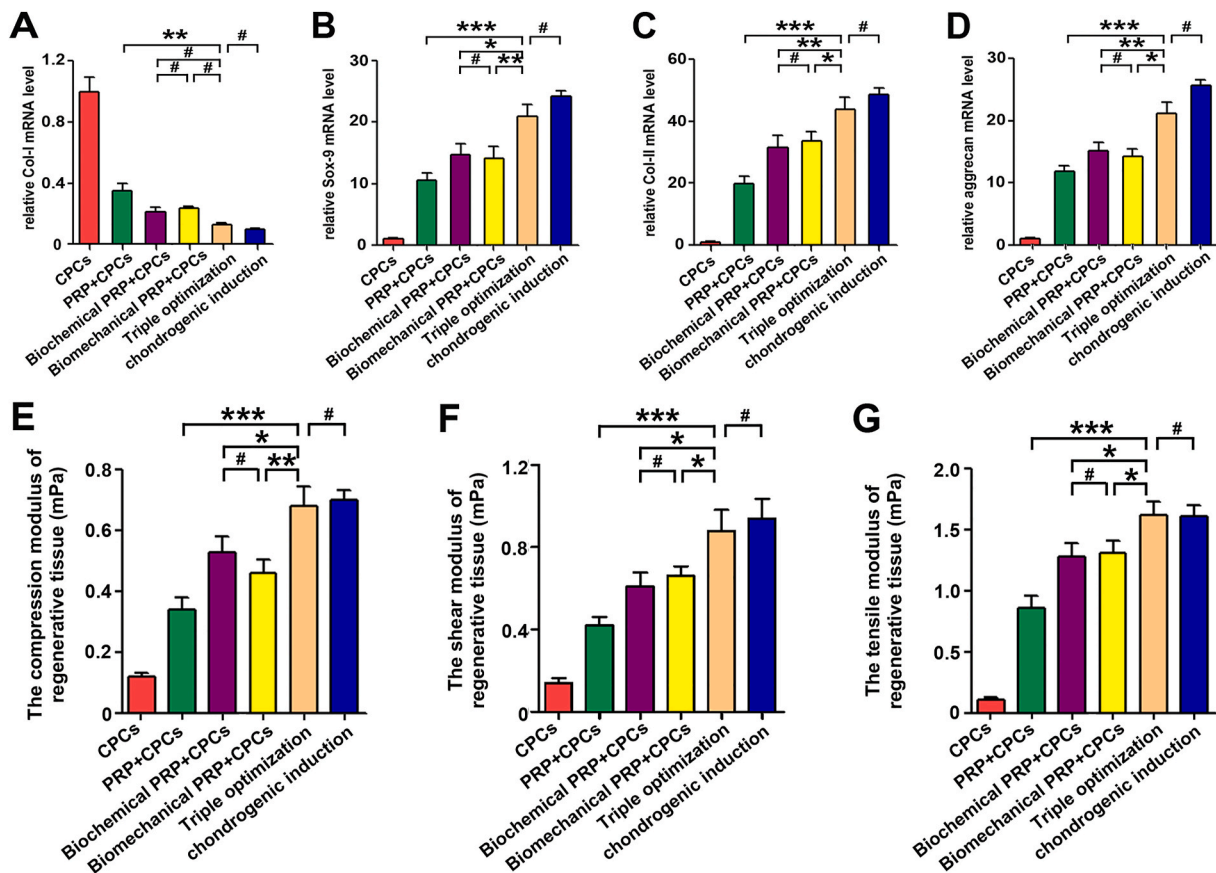


Fig. 9. Gene expression and biomechanical properties of the regenerated tissues after 12 weeks *in vivo*. (A–D) Expression of Col-I, Sox-9, Col-II, and aggrecan genes in regenerated tissue 12 weeks after *in vivo* implantation. (E–G) Biomechanical properties of the regenerated cartilage 12 weeks after *in vivo* implantation. Data are presented as mean \pm SEM, $n = 3$, $*P < 0.05$, $**P < 0.01$, $***P < 0.001$ and $\#P > 0.05$.

that of other frequently used cell sources, including MSCs and chondrocytes, in PRP-based cartilage regeneration and found that CPCs were a superior alternative for cartilage engineering [19]. In the present study, we prepared CPCs using a method to collect migrating cells from full-thickness cartilage pieces and further characterized them with tri-lineage differentiation and migration/chemotaxis assays. The strong chondrogenesis of CPCs and the high synthesis of chondrogenic-related proteins potentially provided evidence that CPCs were favorable to be applied as a cell resource in the PRP-based cartilage tissue engineering.

Several studies reported that PRPs with different platelet concentrations exerted discriminatory effects on cell behavior, especially guiding them toward different cell fate [16]; thus, optimization of the platelet concentration is crucial for PRP-based construct application. In the present study, we detected the chondrogenic differentiation of CPCs cocultured with PRPs at different concentrations and found that PRPs with different concentrations of platelets exerted different effects on proliferation and chondrogenesis of CPCs, which may be because that the concentration gradient of growth factors in PRP affects the cellular functions of CPCs. Ultimately, we found that PRPs with platelet concentrations of 3000×10^9 pl/L $\sim 4000 \times 10^9$ pl/L exerted the highest efficacy to encourage CPCs toward chondrogenesis, which could be selected as favorable PRPs for applications in optimized PRP + CPC constructs. The various effects occurred partly due to the different doses and components of the growth factor cocktails, which probably activated some implicated signal pathways in the process of CPC chondrogenesis [17]. However, the related microenvironmental signals involved in administrating the discrepant fate of CPCs by PRPs should be further investigated to reinforce these findings.

Cartilage architecture and biomechanical composition are strictly regulated by cell sources in response to changes in their chemical and mechanical environment [42]. Natural PRP-based gels consisting of physically crosslinked networks have poor mechanical properties, whereas the PRP gels assisted by a proper cocktail of thrombin and CaCl_2 produced a more stable chemical force and adequate fibrin crosslinking, thus exhibiting good mechanical performance. The aforementioned higher G' value, later crossover point, as well as greater tensile, compressive, and shear moduli in 10% CaCl_2 -40 U/ml BT-treated gels collectively supported that PRP gels treated with the cocktail of 10% CaCl_2 -40 U/ml BT possessed a better mechanical performance. Mechanistically, the outperformed biomechanical property may be partly attributed to the strengthened crosslinking induced by a higher density of reversible hydrogen bond interactions caused by 40 U/ml BT [43]. Additionally, the fibrin monomer bound by hydrogen bonds could be further immobilized by forming bridge bonds between adjacent peptide chains after the gel was treated with 10% CaCl_2 [44]. Thus, the double-crosslinked and stable fibrin polymer mediates the transition of the PRP gel from a predominantly physical crosslinked network to a more chemically crosslinked network and greatly improving both the strength and elasticity of PRP gels [32,45]. However, excessive crosslinking formed by thrombin at 80 U/ml may lead to the overextension of fibrin and a loss of internal mechanical storage of the network [43]. Furthermore, residual calcium in PRP gel treated with 15% Ca^{2+} could induce protein crystallization, which may contribute to the decreased viscoelasticity [46,47].

In this study, the triple-optimization process imposed on PRP constructs produced a significant increase in the regeneration of cartilage compared with the single-, dual-optimizations, or sole CPC treatment. The mechanism may be related to the growth factors with appropriate concentration dominating the microenvironment and the reinforced strength of fibrin provided for tissue reconstruction, which provides favorable 3-D microenvironmental support for CPC migration, proliferation, and differentiation both chemically and mechanically. In details, the optimization of platelet concentration provides a suitable growth factor cocktail for establishing a favorable biological environment to induce CPCs toward the chondrogenic lineage and stimulate accumulation of ECM. Furthermore, the optimized bioscaffold with a

μm -scale porous morphology offers a conductive 3-D structure and contact guidance for CPC migration, stretch, and survival. In addition, the reinforced biomechanics of PRP constructs provide a more stable and stronger structure in the provisional scaffold, which creates stronger support initializing the tissue repair process and evolving PRP gel for tissue regeneration. Given that connective tissues are known to derive the biomechanical properties from their biochemical constituents, the higher synthesis of chondrogenic-related protein and the improved cartilaginous matrix deposition induced by appropriate growth factors and sufficient mechanics within the triple-optimization construct may be primarily responsible for the improved tensile and compressive moduli of the regenerated tissues [48–50].

The contribution of implanted cells to generate reparative cartilage is a critical issue, and the elucidation of which may enable us to better understand the mechanisms of PRP-based cartilage tissue engineering. Xie et al. used PRP loaded EGFP-labeled ADSCs to treat cartilage defects and found that implanted ADSCs changed into chondrocyte-like cells with accumulation of matrix Col II, implying the dominant role of implanted cells in cartilage regeneration *in vivo* [29]. Yoshioka et al. tracked MSCs labeled with i-QDs in the reparative tissue, and demonstrated that MSCs indeed contributed to the regeneration of osteochondral defects through differentiation into chondrocytes [51]. Zhou et al. used GFP-labeled BMSCs and biodegradable polymers to repair articular osteochondral defects, and found that GFP-labeled cells were more detected in the engineered cartilage than unlabeled cells [52]. These results strongly indicate that the implanted seeding cells can differentiate into chondrocyte-like cells and generate engineered cartilage during the process of cartilage regeneration. In addition, previous studies showed that chondrocytes possessed poor proliferative potential even post the stimulation of PRP while CPCs responded more strongly to the PRP stimulation than chondrocytes and possessed strong proliferation. Therefore, we speculate that it is the *in situ* proliferation and chondrogenesis of CPCs rather than the ingrowth to the gels of outside chondrocytes that accounts for the chondrocyte regeneration.

However, we must acknowledge that there are limitations in this study. Although, we found that the PRP + CPC constructs generated better cartilage regeneration than those of the untreated groups, the experiments as designed did not rule out a possibility of stimulated ingrowth of outside chondrocytes to the gels. Therefore, cell tracking assay should be performed to investigate the fate of the transplanted CPCs in PRP scaffolds. In addition, considering that MSCs in a PRP gel has potential for bone regeneration and can serve as a viable clinical alternative to repair of bone defect, we may expand the depth of modeling and employ MSCs together with CPCs in this triple-optimized PRP construct to observe the repair efficacy on osteochondral defects. Angiogenesis is an essential factor in wound healing, thus the vascular and angiogenesis expression in cartilage defect site should be further investigated to capture a better understanding of regenerative process of tissues. In the current study, CPCs were seeded in 48-well culture plates for chondrogenic differentiation to select the optimal platelet concentration. Considering that there may exist a distinction between two-dimensional culture conditions and three-dimensional culture conditions, subsequent experiments are needed to further verify the results conducted in two-dimensional culture conditions. In the animal studies, only the results of 12 weeks post-operation were tested, which may obscure the regenerative process at an earlier stage. Thus, further work is necessary to evaluate the efficacy of the triple-optimized PRP + CPC construct at different stages of tissue regeneration. Furthermore, in most of the *in vitro* experiments, the effect of optimized PRP on CPCs differentiation was mainly presented by mRNA expression, which was inferior to detecting the protein expression level for drawing conclusion. Further studies such as western-blotting analysis can be performed to validate these data.

5. Conclusions

In this study, we developed an orchestrated three-step tissue engineering strategy for fabricating PRP + CPC constructs by employing CPCs as a cell resource, optimizing platelet concentration, and adding an enzyme-ion activator. This triple-optimized construct was demonstrated to significantly promote cartilage regeneration in both structural reconstruction and biomechanical recovery. This work demonstrates the efficacy of triple-optimization strategy to design cartilage tissue engineering scaffolds and highlights the feasibility of this triple-optimization PRP + CPC construct for cartilage regeneration.

CRedit authorship contribution statement

Ketao Wang: Writing – original draft, Data curation, Investigation, Methodology, Software. **Ji Li:** Writing – original draft, Data curation, Visualization. **Yuxing Wang:** Investigation, Methodology, Visualization. **Yaqiang Wang:** Data curation, Software, Methodology. **Yuanyuan Qin:** Methodology, Investigation. **Fei Yang:** Formal analysis, Supervision, Validation, Writing – review & editing. **Mingzhu Zhang:** Investigation, Methodology, Data curation, Writing – review & editing, Funding acquisition, Supervision, Conceptualization, Resources. **Heng Zhu:** Formal analysis, Validation, Supervision, Funding acquisition, Writing – review & editing. **Zhongli Li:** Conceptualization, Project administration, Resources, Funding acquisition, Supervision, Writing – review & editing.

Declaration of competing interest

We declare that we do not have any competing financial interest in the work submitted.

Acknowledgments

The authors thank Yimeng Yang, Chunhui Liu, and Hongtao Yang for assistance with statistical analysis and critical revision of the manuscript. The authors also thank Prof. Haibao Wang for preparing the whole blood samples. This study was supported by the National Natural Science Foundation of China (81871771, 81572159) and the Beijing Natural Sciences Grants (7182123, 7191010).

Appendix A. Supplementary data

Supplementary data to this article can be found online at <https://doi.org/10.1016/j.bioactmat.2021.03.037>.

References

- [1] A.R. Armiento, M.J. Stoddart, M. Alini, D. Eglin, Biomaterials for articular cartilage tissue engineering: learning from biology, *Acta Biomater.* 65 (2018) 1–20.
- [2] B.J. Huang, J.C. Hu, K.A. Athanasiou, Cell-based tissue engineering strategies used in the clinical repair of articular cartilage, *Biomaterials* 98 (2016) 1–22.
- [3] T. Novak, B. Seelbinder, C.M. Twitchell, C.C. van Donkelaar, S.L. Voytik-Harbin, C. P. Neu, Mechanisms and microenvironment investigation of cellularized high density gradient collagen matrices via densification, *Adv. Funct. Mater.* 26 (16) (2016) 2617–2628.
- [4] F. Gao, Z. Xu, Q. Liang, H. Li, L. Peng, M. Wu, X. Zhao, X. Cui, C. Ruan, W. Liu, Osteochondral regeneration with 3D-printed biodegradable high-strength supramolecular polymer reinforced-gelatin hydrogel scaffolds, *Advanced science (Weinheim, Baden-Wuerttemberg, Germany)* 6 (15) (2019) 1900867.
- [5] V.P. Ribeiro, A. da Silva Morais, F.R. Maia, R.F. Canadas, J.B. Costa, A.L. Oliveira, J.M. Oliveira, R.L. Reis, Combinatory approach for developing silk fibroin scaffolds for cartilage regeneration, *Acta Biomater.* 72 (2018) 167–181.
- [6] X. Xie, C. Zhang, R.S. Tuan, Biology of platelet-rich plasma and its clinical application in cartilage repair, *Arthritis Res. Ther.* 16 (1) (2014) 204.
- [7] T.E. Foster, B.L. Puskas, B.R. Mandelbaum, M.B. Gerhardt, S.A. Rodeo, Platelet-rich plasma: from basic science to clinical applications, *Am. J. Sports Med.* 37 (11) (2009) 2259–2272.
- [8] S.P. Grogan, S. Miyaki, H. Asahara, D.D. D’Lima, M.K. Lotz, Mesenchymal progenitor cell markers in human articular cartilage: normal distribution and changes in osteoarthritis, *Arthritis Res. Ther.* 11 (3) (2009) R85.
- [9] W. Ando, K. Tateishi, D.A. Hart, D. Katakai, Y. Tanaka, K. Nakata, J. Hashimoto, H. Fujie, K. Shino, H. Yoshikawa, N. Nakamura, Cartilage repair using an in vitro generated scaffold-free tissue-engineered construct derived from porcine synovial mesenchymal stem cells, *Biomaterials* 28 (36) (2007) 5462–5470.
- [10] D. Kardos, I. Hornyak, M. Simon, A. Hinsenkamp, B. Marschall, R. Vardai, A. Kallay-Menyhard, B. Pinke, L. Meszaros, O. Kuten, S. Nehrer, Z. Lacza, Biological and mechanical properties of platelet-rich fibrin membranes after thermal manipulation and preparation in a single-syringe closed system, *Int. J. Mol. Sci.* 19 (11) (2018).
- [11] T.W. Chow, L.V. McIntire, D.M. Peterson, Importance of plasma fibronectin in determining PFP and PRP clot mechanical properties, *Thromb. Res.* 29 (2) (1983) 243–248.
- [12] M. Sadeghi-Ataabad, Z. Mostafavi-Pour, Z. Vojdani, M. Sani, M. Latifi, T. Talaei-Khozani, Fabrication and characterization of platelet-rich plasma scaffolds for tissue engineering applications, *Materials science & engineering, C, Materials for biological applications* 71 (2017) 372–380.
- [13] R.F. LaPrade, L.R. Goodrich, J. Phillips, G.J. Dornan, T.L. Turnbull, M.L. Hawes, K. D. Dahl, A.N. Coggins, J. Kisiday, D. Frisbie, J. Chahla, Use of platelet-rich plasma immediately after an injury did not improve ligament healing, and increasing platelet concentrations was detrimental in an in vivo animal model, *Am. J. Sports Med.* 46 (3) (2018) 702–712.
- [14] O. Wahlstrom, C. Linder, A. Kalen, P. Magnusson, Variation of pH in lysed platelet concentrates influence proliferation and alkaline phosphatase activity in human osteoblast-like cells, *Platelets* 18 (2) (2007) 113–118.
- [15] Z. Badran, M.N. Abdallah, J. Torres, F. Tamimi, Platelet concentrates for bone regeneration: current evidence and future challenges, *Platelets* 29 (2) (2018) 105–112.
- [16] K. Wang, Z. Li, J. Li, W. Liao, Y. Qin, N. Zhang, X. Huo, N. Mao, H. Zhu, Optimization of the platelet-rich plasma concentration for mesenchymal stem cell applications, *tissue engineering, Part. A*. 25 (5–6) (2019) 333–351.
- [17] S. Koelling, J. Kruegel, M. Irmer, J.R. Path, B. Sadowski, X. Miro, N. Miosge, Migratory chondrogenic progenitor cells from repair tissue during the later stages of human osteoarthritis, *Cell stem cell* 4 (4) (2009) 324–335.
- [18] G.P. Dowthwaite, J.C. Bishop, S.N. Redman, I.M. Khan, P. Rooney, D.J. Evans, L. Haughton, Z. Bayram, S. Boyer, B. Thomson, M.S. Wolfe, C.W. Archer, The surface of articular cartilage contains a progenitor cell population, *J. Cell Sci.* 117 (Pt 6) (2004) 889–897.
- [19] K. Wang, J. Li, Z. Li, B. Wang, Y. Qin, N. Zhang, H. Zhang, X. Su, Y. Wang, H. Zhu, Chondrogenic progenitor cells exhibit superiority over mesenchymal stem cells and chondrocytes in platelet-rich plasma scaffold-based cartilage regeneration, *Am. J. Sports Med.* 47 (9) (2019) 2200–2215.
- [20] L. Li, Y. Zuo, Q. Zou, B. Yang, L. Lin, J. Li, Y. Li, Hierarchical structure and mechanical improvement of an n-HA/GCO-PU composite scaffold for bone regeneration, *ACS Appl. Mater. Interfaces* 7 (40) (2015) 22618–22629.
- [21] K. Isobe, T. Watanebe, H. Kawabata, Y. Kitamura, T. Okudera, H. Okudera, K. Uematsu, K. Okuda, K. Nakata, T. Tanaka, T. Kawase, Mechanical and degradation properties of advanced platelet-rich fibrin (A-PRF), concentrated growth factors (CGF), and platelet-poor plasma-derived fibrin (PPTF), *International journal of implant dentistry* 3 (1) (2017) 17.
- [22] H.H. Versteeg, J.W. Heemskerk, M. Levi, P.H. Reitsma, New fundamentals in hemostasis, *Physiol. Rev.* 93 (1) (2013) 327–358.
- [23] J.W. Weisel, R.I. Litvinov, Mechanisms of fibrin polymerization and clinical implications, *Blood* 121 (10) (2013) 1712–1719.
- [24] D. Sinha, F.S. Seaman, P.N. Walsh, Role of calcium ions and the heavy chain of factor XIa in the activation of human coagulation factor IX, *Biochemistry* 26 (13) (1987) 3768–3775.
- [25] T. Koklic, R. Majumder, B.R. Lentz, Ca²⁺ switches the effect of PS-containing membranes on Factor Xa from activating to inhibiting: implications for initiation of blood coagulation, *Biochem. J.* 462 (3) (2014) 591–601.
- [26] F.I. Ataullakhanov, R.I. Volkova, A.V. Pokhilko, E.I. Sinauridze, [Threshold behavior of the blood coagulation system upon changes in calcium concentration], *Biofizika* 39 (4) (1994) 713–720.
- [27] M. Ranby, T. Gøjceta, K. Gustafsson, K.M. Hansson, T.L. Lindahl, Isocitrate as calcium ion activity buffer in coagulation assays, *Clin. Chem.* 45 (8 Pt 1) (1999) 1176–1180.
- [28] F.I. Ataullakhanov, A.V. Pohilko, E.I. Sinauridze, R.I. Volkova, Calcium threshold in human plasma clotting kinetics, *Thromb. Res.* 75 (4) (1994) 383–394.
- [29] X. Xie, Y. Wang, C. Zhao, S. Guo, S. Liu, W. Jia, R.S. Tuan, C. Zhang, Comparative evaluation of MSCs from bone marrow and adipose tissue seeded in PRP-derived scaffold for cartilage regeneration, *Biomaterials* 33 (29) (2012) 7008–7018.
- [30] A.M. Nguyen, M.E. Levenston, Comparison of osmotic swelling influences on meniscal fibrocartilage and articular cartilage tissue mechanics in compression and shear, *J. Orthop. Res. : official publication of the Orthopaedic Research Society* 30 (1) (2012) 95–102.
- [31] Z. Yuan, S. Liu, C. Hao, W. Guo, S. Gao, M. Wang, M. Chen, Z. Sun, Y. Xu, Y. Wang, J. Peng, M. Yuan, Q.Y. Guo, AMECM/DCB scaffold prompts successful total meniscus reconstruction in a rabbit total meniscectomy model, *Biomaterials* 111 (2016) 13–26.
- [32] A. Vedadghavami, F. Minooei, M.H. Mohammadi, S. Khetani, A. Rezaei Kolahchi, S. Mashayekhan, A. Sanati-Nezhad, Manufacturing of hydrogel biomaterials with controlled mechanical properties for tissue engineering applications, *Acta Biomater.* 62 (2017) 42–63.
- [33] O. Chaudhuri, J. Cooper-White, P.A. Janmey, D.J. Mooney, V.B. Shenoy, Effects of extracellular matrix viscoelasticity on cellular behaviour, *Nature* 584 (7822) (2020) 535–546.

- [34] H. Zhu, Z.K. Guo, X.X. Jiang, H. Li, X.Y. Wang, H.Y. Yao, Y. Zhang, N. Mao, A protocol for isolation and culture of mesenchymal stem cells from mouse compact bone, *Nat. Protoc.* 5 (3) (2010) 550–560.
- [35] V. Deshmukh, H. Hu, C. Barroga, C. Bossard, S. Kc, L. Dellamary, J. Stewart, K. Chiu, M. Ibanez, M. Pedraza, T. Seo, L. Do, S. Cho, J. Cahiwat, B. Tam, J.R. S. Tambiah, J. Hood, N.E. Lane, Y. Yazici, A small-molecule inhibitor of the Wnt pathway (SM04690) as a potential disease modifying agent for the treatment of osteoarthritis of the knee, *Osteoarthritis Cartilage* 26 (1) (2018) 18–27.
- [36] S.P. Grogan, A. Barbero, V. Winkelmann, F. Rieser, J.S. Fitzsimmons, S. O'Driscoll, I. Martin, P. Mainil-Varlet, Visual histological grading system for the evaluation of in vitro-generated neocartilage, *Tissue Eng.* 12 (8) (2006) 2141–2149.
- [37] J.L. Guo, Y.S. Kim, E.A. Orchard, J. van den Beucken, J.A. Jansen, M.E. Wong, A. G. Mikos, A rabbit femoral condyle defect model for assessment of osteochondral tissue regeneration, *tissue engineering, Part C, Methods* 26 (11) (2020) 554–564.
- [38] M.P. van den Borne, N.J. Rajmakers, J. Vanlauwe, J. Victor, S.N. de Jong, J. Bellemans, D.B. Saris, International cartilage repair society (ICRS) and oswestry macroscopic cartilage evaluation scores validated for use in autologous chondrocyte implantation (ACI) and microfracture, *Osteoarthritis Cartilage* 15 (12) (2007) 1397–1402.
- [39] X. Chen, I.A. Jones, C. Park, C.T. Vangsness Jr., The efficacy of platelet-rich plasma on tendon and ligament healing: a systematic review and meta-analysis with bias assessment, *Am. J. Sports Med.* 46 (8) (2018) 2020–2032.
- [40] R. Langer, J.P. Vacanti, *Tissue engineering*, *Science* 260 (5110) (1993) 920–926.
- [41] Z. Luo, S. Zhang, J. Pan, R. Shi, H. Liu, Y. Lyu, X. Han, Y. Li, Y. Yang, Z. Xu, Y. Sui, E. Luo, Y. Zhang, S. Wei, Time-responsive osteogenic niche of stem cells: a sequentially triggered, dual-peptide loaded, alginate hybrid system for promoting cell activity and osteo-differentiation, *Biomaterials* 163 (2018) 25–42.
- [42] M. Qasim, D.S. Chae, N.Y. Lee, Bioengineering strategies for bone and cartilage tissue regeneration using growth factors and stem cells, *J. Biomed. Mater. Res.* 108 (3) (2020) 394–411.
- [43] M.W. Mosesson, Fibrinogen and fibrin structure and functions, *J. Thromb. Haemostasis : JTH* 3 (8) (2005) 1894–1904.
- [44] J. Yan, F. Chen, B.G. Amsden, Cell sheets prepared via gel-sol transition of calcium RGD-alginate, *Acta Biomater.* 30 (2016) 277–284.
- [45] M. Pensalfini, A.E. Ehret, S. Studeli, D. Marino, A. Kaeck, E. Reichmann, E. Mazza, Factors affecting the mechanical behavior of collagen hydrogels for skin tissue engineering, *Journal of the mechanical behavior of biomedical materials* 69 (2017) 85–97.
- [46] D. Serp, M. Mueller, U. Von Stockar, I.W. Marison, Low-temperature electron microscopy for the study of polysaccharide ultrastructures in hydrogels. II. Effect of temperature on the structure of Ca²⁺-alginate beads, *Biotechnol. Bioeng.* 79 (3) (2002) 253–259.
- [47] R. Willaert, I. Zegers, L. Wyns, M. Sleutel, Protein crystallization in hydrogel beads, *Acta crystallographica, Section D, Biological crystallography* 61 (Pt 9) (2005) 1280–1288.
- [48] W.M. Han, S.J. Heo, T.P. Driscoll, J.F. Delucca, C.M. McLeod, L.J. Smith, R. L. Duncan, R.L. Mauck, D.M. Elliott, Microstructural heterogeneity directs micromechanics and mechanobiology in native and engineered fibrocartilage, *Nat. Mater.* 15 (4) (2016) 477–484.
- [49] Z.Z. Zhang, Y.R. Chen, S.J. Wang, F. Zhao, X.G. Wang, F. Yang, J.J. Shi, Z.G. Ge, W. Y. Ding, Y.C. Yang, T.Q. Zou, J.Y. Zhang, J.K. Yu, D. Jiang, Orchestrated biomechanical, structural, and biochemical stimuli for engineering anisotropic meniscus, *Sci. Transl. Med.* 11 (487) (2019).
- [50] S. Glyn-Jones, A.J. Palmer, R. Agricola, A.J. Price, T.L. Vincent, H. Weinans, A. J. Carr, Osteoarthritis, *Lancet (London, England)* 386 (9991) (2015) 376–387.
- [51] T. Yoshioka, H. Mishima, Z. Kaul, Y. Ohyabu, S. Sakai, N. Ochiai, S.C. Kaul, R. Wadhwa, T. Uemura, Fate of bone marrow mesenchymal stem cells following the allogeneic transplantation of cartilaginous aggregates into osteochondral defects of rabbits, *Journal of tissue engineering and regenerative medicine* 5 (6) (2011) 437–443.
- [52] G. Zhou, W. Liu, L. Cui, X. Wang, T. Liu, Y. Cao, Repair of porcine articular osteochondral defects in non-weightbearing areas with autologous bone marrow stromal cells, *Tissue Eng.* 12 (11) (2006) 3209–3221.